

Accepted Manuscript

International Journal of Structural Stability and Dynamics

Article Title: Periodic Response and Stability of a Maglev System with Delayed Feedback Control Under Aerodynamic Lift

Author(s): Han Wu, Xiao-Hui Zeng, Ding-Gang Gao

DOI: 10.1142/S0219455421500401

Received: 02 September 2020

Accepted: 18 November 2020

To be cited as: Han Wu, Xiao-Hui Zeng, Ding-Gang Gao, Periodic Response and Stability of a Maglev System with Delayed Feedback Control Under Aerodynamic Lift, *International Journal of Structural Stability and Dynamics*, doi: 10.1142/S0219455421500401

Link to final version: <https://doi.org/10.1142/S0219455421500401>

This is an unedited version of the accepted manuscript scheduled for publication. It has been uploaded in advance for the benefit of our customers. The manuscript will be copyedited, typeset and proofread before it is released in the final form. As a result, the published copy may differ from the unedited version. Readers should obtain the final version from the above link when it is published. The authors are responsible for the content of this Accepted Article.

Periodic Response and Stability of a Maglev System with Delayed Feedback Control Under Aerodynamic Lift

Han Wu^{a,b}, Xiao-Hui Zeng^{a,b,1}, Ding-Gang Gao^c

^a *Key Laboratory for Mechanics in Fluid Solid Coupling Systems, Institute of Mechanics, Chinese Academy of Sciences, Beijing, China*

^b *School of Engineering Science, University of Chinese Academy of Sciences, Beijing, China*

^c *Maglev Transportation Engineering R&D Center, Tongji University, Shanghai, China*

Abstract:

In this research, the periodic response and stability of a nonlinear maglev system under the combined effects of steady and unsteady aerodynamic lifts is investigated, considering time delay in the feedback control loop. Firstly, a nonlinear maglev system with a single levitation point that accounts for the nonlinearity of the electromagnetic force, time delay in the feedback control loop, and effect of aerodynamic lift is established. Then, the periodic solutions of the maglev system with aerodynamic lift and time delays are obtained by an incremental harmonic balance analysis, in which the explicit time-delay action matrices used indicate that the effect of time delay on the response of the maglev system is periodic. The stability of the periodic solutions based on a finite difference continuous time approximation method and Floquet theory is studied, from which the critical time delay is obtained. Also examined is the relationship between the periodic vibration amplitude and the time delay, steady aerodynamic lift coefficient, and frequency of the unsteady aerodynamic lift, as well as the variation of critical delay with respect to the position feedback and velocity feedback with the control gain parameters. In addition, the stability boundary for the simultaneous time-delayed position and velocity feedback is obtained.

¹ Corresponding author. *E-mail address:* zXH@imech.ac.cn (Xiao-Hui Zeng)

Key Words: Maglev vehicle, Aerodynamic lift, Time delay, Incremental harmonic balance, Periodic response, Stability.

1 Introduction

Electromagnetic suspension (EMS) trains have the advantages of low energy consumption, low environmental impacts, low noise, low maintenance, and strong climbing abilities, and they have undergone tremendous development in recent years. The dynamic characteristics of maglev train are important to its application, and many scholars have studied it in recent years [1, 2]. The new generation of high-speed maglev trains will have design speeds reaching 600 km/h, which exceeds the cruising speed of low-speed aircraft, and their aerodynamic loads will have a non-negligible effect on their dynamic behaviors during high-speed maglev operation. In recent years, more and more researchers have begun focusing on the aerodynamic loads of high-speed maglev trains and they have analyzed the aerodynamic loads and pressure waves of maglev train operating in open air, passing other trains, and other situations [3–7]. However, the dynamic responses of maglev trains subjected to aerodynamic loads have rarely been studied. Kwon et al. [8] simulated the responses of maglev vehicles when they passed a suspension bridge and they were subjected to wind gusts. Yau [9] considered the aerodynamic load caused by unstable airflow and calculated the response of a coupled vehicle-rails system. Wu and Shi [10] analyzed the dynamic response of a maglev vehicle body under the action of a wind field. The current research on the dynamics of maglev vehicles under aerodynamic conditions mainly uses simulation methods to study the motion responses and stability under various operating conditions, but these simulations do not account for the vibration characteristics, such as the stability and nonlinear response characteristics of maglev vehicles.

The levitation stability of an EMS-

type maglev vehicle relies on a controlled vertical electromagnetic force. Compared to aerodynamic forces in the other directions, the vertical aerodynamic force, or aerodynamic lift, has the most direct effect on the dynamic characteristics of a maglev train. Using a train for the Shanghai Maglev Line as an example, numerical calculations showed that for a running speed of 600 km/h, the aerodynamic lift of the lead car could reach 50% of the vehicle weight [4]. There has been an industrial consensus in the design of control systems for high-speed maglev trains that the effect of aerodynamic lift must be taken into account. A steady aerodynamic lift changes the equilibrium state of a maglev train; as the vehicle speed increases, the train may become unstable. Therefore, there is a critical speed due to the aerodynamic lift. We have previously investigated the destabilization mechanism of maglev vehicles under steady aerodynamic lift, proposed the concept of a critical speed, and summarized two instability modes for steady aerodynamic lift [11].

In addition to the steady aerodynamic lift during the high-speed operation of maglev trains, the development of unstable vortices around a train causes pronounced unsteady aerodynamic lift [4]. To ensure the safe and comfortable operation of maglev trains in the presence of aerodynamic lift and to provide a basis for the design of a control system, in this study, we investigated the dynamic characteristics of maglev trains under the combined action of steady and unsteady aerodynamic lift based on the results of previous studies.

A maglev train is a nonlinear system that integrates mechanics, control, power, and electronics, with the electromagnetic nonlinearity being one of the most important nonlinearities. Furthermore, time delays are inevitable in the measurement and reception of signals and in the processing, output, and execution of signals. The existence of time delays will cause changes in the dynamic behavior of a maglev system and it may even cause a system to become unstable. In real vehicle tests, there have been cases of violent vehicle-guideway resonance caused by excessive time delays in a control loop [12, 13]. To address the effect of

time delays on the stability of maglev vehicles, Li et al. [14] analyzed the effects of time delays on the stability of a coupled vehicle-guideway system. Wan et al. [15–17] considered the effects of delayed position feedback control and velocity feedback control on the Hopf bifurcations and resonance problems of maglev systems. Zhan et al. [18–22] discussed the effects of time delays on the stability and Hopf bifurcations of rigid-guideway and elastic-guideway maglev vehicles. Xu et al. [13] studied the Hopf bifurcation problem of coupled vehicle-rails systems with simultaneous time delays in position and speed feedback. Sun et al. [23] studied the interaction and constraint of time-delay parameters on the Hopf bifurcation of a low-speed maglev vehicle. Sun et al. [24] proposed an adaptive robust controller based on the Riccati method and sliding-mode technology when a time delay was considered.

Previous research studies on maglev vehicle systems have either not considered the influence of aerodynamic lift or they have only considered aerodynamic loads in multiple directions to analyze their equality. The suspension stability of a maglev train is the most important, and the influence of aerodynamic lift on the suspension stability is the most direct of all aerodynamic loads. To date, there has not been any relevant research on the suspension stability characteristics of a maglev vehicle under aerodynamic lift. In addition, previous research on time-delayed maglev train systems has mainly focused on Hopf bifurcations instead of the dynamic response under external excitation, especially the excitation of aerodynamic lift. When a train is running at a very high speed, it is an extremely important problem to determine whether the response characteristics of the maglev vehicle system with time delay under unsteady aerodynamic lift can meet the control requirements. However, no researchers have studied the nonlinear dynamic characteristics of maglev systems associated with the aerodynamic lift effect and time delays in the feedback control loop. This paper describes the first research to examine the periodic response and its stability for a maglev system under the action of both unsteady aerodynamic lift and time delay. Many kinds of loads during the

operation of train can be regarded as harmonic excitation to some extent, and the periodic response is important content of vehicle dynamics [25]. In this study, we took the nonlinear electromagnetic forces and time delays in the position and velocity feedback control loop into account and we established a single-magnet suspension nonlinear maglev system that considered the steady and unsteady aerodynamic lift with simple harmonic variations. Based on the incremental harmonic balance (IHB) method, we analyzed the periodic solutions of maglev systems and we investigated the stability of the periodic solution based on a finite difference continuous time approximation method and the Floquet theory. We analyzed the relationship between the periodic solution amplitude and the time delay as well as the aerodynamic lift fluctuation frequency. We also considered the relationship between the critical velocity feedback, the position feedback time delays, and the control gain parameters. In addition, the delayed stability boundaries when the position feedback and velocity feedback time delays were considered simultaneously were investigated in this study. These findings are important for revealing the suspension stability characteristics of a high-speed maglev vehicle system.

2 System Model and Dynamic Equations

To clearly describe the mechanism for the influence of aerodynamic lift on the suspension dynamic stability of a maglev system, we began the investigation using the single-magnet suspension control model shown in Figure 1. In this model, the maglev was simplified to one electromagnet, only the vertical vibration and vertical electromagnetic force of the electromagnet were taken into account, and the rotation motion and electromagnetic torque were ignored. The guideway was considered to be rigid. In the figure, F represents the electromagnetic force, F_{Lift} represents the aerodynamic lift, δ represents the suspension clearance of the electromagnet, and v represents the vehicle speed.

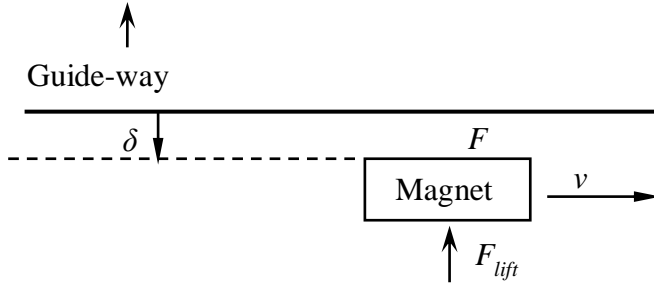


Figure 1 Schematic diagram of a single-magnet suspension system

Since the unstable vortex of the train was periodic, we regarded the unsteady aerodynamic lift in this study as harmonic. Considering the oncoming airflow of the maglev train, the steady and unsteady aerodynamic lift forces acting on the vehicle could be expressed as

$$\begin{aligned}
 F_L &= F_{L0} + F_{L\Delta} \\
 F_{L0} &= \frac{1}{2} C_L \rho A_v v^2 \\
 F_{L\Delta} &= H \sin(2\pi f \cdot t)
 \end{aligned} \tag{1}$$

where F_L is the aerodynamic lift, F_{L0} is the steady aerodynamic lift, $F_{L\Delta}$ is the unsteady aerodynamic lift, C_L is the steady aerodynamic lift coefficient, ρ is the density of air (1.225 kg/m^3), A_v is the vehicle top surface area of the vehicle, v is the headwind velocity (i.e., the vehicle speed), f is the frequency of the unsteady aerodynamic lift, and H is the amplitude of the unsteady aerodynamic lift.

The maglev system had an equilibrium state that was denoted as (I_0, δ_0) , where the electromagnetic force was equal to the sum of gravity and the steady aerodynamic lift. I_0 was the equilibrium current and δ_0 was the equilibrium clearance. Furthermore, i denoted the fluctuation of the current with respect to the equilibrium current, and s denoted the fluctuation of the suspension clearance of the electromagnet with respect to the equilibrium clearance. Then the suspension force between the electromagnet and the guide-way could be written as

$$F = \frac{\mu_0 AN^2 (I_0 + i)^2}{4(\delta_0 + s)^2} \tag{2}$$

where μ_0 is the magnetic permeability of air, A is the effective area of the electromagnet, and N is the number

berofturnsinthecoil.

ExpandingtheaboveformulaasaTaylorseries,weobtained

$$F = \frac{\mu_0 AN^2}{4\delta_0^2} (I_0^2 + 2I_0 i + i^2) \left[1 + 2 \left(-\frac{s}{\delta_0} \right)^1 + 3 \left(-\frac{s}{\delta_0} \right)^2 + 4 \left(-\frac{s}{\delta_0} \right)^3 L \right] \quad (3)$$

Thecurrentwascontrolledbyaproportional-differential(PD)controller,andthetime-delayinthepositionandvelocityfeedbackcontrolloopwastakenintoaccount.Then,the fluctuationof thecurrent*i*wasexpressedas

$$i = k_p \cdot s(t - t_p) + k_d \cdot \dot{\mathcal{E}}(t - t_d), \quad (4)$$

where*k_p*and*k_d*arethegainsofthe positionfeedbackcontrolandthe velocityfeedbackcontrol, respectively, and*t_p*and*t_d*arethetimedelays ofthe positionfeedbackandthe velocityfeedback, respectively.

SubstitutingEq.(4)intoEq.(3)andkeepingtermswithsecond-orderprecision,wehad

$$F = \frac{\mu_0 AN^2}{4\delta_0^2} \left(I_0^2 + 2I_0 [k_p \cdot s_p + k_d \cdot \dot{\mathcal{E}}] + [k_p \cdot s_p + k_d \cdot \dot{\mathcal{E}}]^2 \right) \cdot \left[1 + 2 \left(-\frac{s}{\delta_0} \right)^1 + 3 \left(-\frac{s}{\delta_0} \right)^2 + 4 \left(-\frac{s}{\delta_0} \right)^3 L \right] \quad (5)$$

Theelectromagneticforceattheequilibriumstatewasexpressedas

$$F_0 = \frac{\mu_0 AN^2}{4\delta_0^2} I_0^2 \quad . \text{Attheequilibriumstate,wehad} \quad F_0 = mg + F_{L0} \quad , \text{then}$$

$$I_0 = \frac{2\delta_0}{N} \sqrt{\frac{mg + F_{L0}}{\mu_0 A}} \quad . \text{Thefluctuationoftheelectromagneticforcewithrespecttotheequilibriumsta}$$

tecouldbederivedas

$$\begin{aligned} \Delta F = F - F_0 = & k_1 \left(k_p s_p - \frac{I_0}{\delta_0} s \right) + k_1 k_d \dot{\mathcal{E}} \\ & + k_2 \left(k_p^2 s_p^2 - \frac{4I_0 k_p}{\delta_0} s s_p + \frac{3I_0^2}{\delta_0^2} s^2 \right) + k_2 \left(2k_p k_d s_p \dot{\mathcal{E}} - \frac{4I_0 k_d}{\delta_0} s \dot{\mathcal{E}} \right) + k_2 (k_d^2) \dot{\mathcal{E}}^2 \end{aligned} \quad (6)$$

$$\text{Intheaboveformula, } k_1 = \frac{2\mu_0 AN^2 I_0}{4\delta_0^2}, k_2 = \frac{\mu_0 AN^2}{4\delta_0^2}, s(t - t_p) = s_p, \dot{\mathcal{E}}(t - t_d) = \dot{\mathcal{E}}.$$

Taking the downward vertical direction as the positive direction, the equation of motion of the magnetic suspension system in the vertical direction with respect to the equilibrium state could be written as

$$m\ddot{x} = F_{L\Delta} - \Delta F, \quad (7)$$

where m is the mass of the electromagnet.

By substituting Eqs. (1) and (6) into Eq. (7), we obtained a nonlinear magnetic levitation model under the combined effect of steady and unsteady aerodynamic lift and the influence of the time delays in the feedback control loops:

$$m\ddot{x} + \mu_{11}s_p + \mu_{12}s + \mu_{21}\dot{x}_d + \mu_{31}s_p^2 + \mu_{32}s s_p + \mu_{33}s^2 + \mu_{41}s_p \dot{x}_d + \mu_{42}s \dot{x}_d + \mu_{51}\dot{x}_d^2 = H \sin(2\pi ft) \quad (8)$$

In the above formula,

$$\begin{aligned} \mu_{11} &= k_1 k_p, \mu_{12} = -k_1 \frac{I_0}{\delta_0}, \mu_{21} = k_1 k_d, \\ \mu_{31} &= k_2 k_p^2, \mu_{32} = -k_2 \frac{4I_0 k_p}{\delta_0}, \mu_{33} = k_2 \frac{3I_0^2}{\delta_0^2}, \\ \mu_{41} &= 2k_2 k_p k_d, \mu_{42} = -k_2 \frac{4I_0 k_d}{\delta_0}, \mu_{51} = k_2 k_d^2, \\ \mu_{61} &= -k_3 k_p^2, \mu_{62} = k_3 \frac{3I_0 k_p}{\delta_0}, \mu_{63} = -k_3 \frac{2I_0^2}{\delta_0^2}, \\ \mu_{71} &= k_3 \frac{3I_0 k_d}{\delta_0}, \mu_{72} = -k_3 2k_p k_d, \mu_{81} = -k_3 k_d^2. \end{aligned}$$

3 IHB Method

For the nonlinear magnetic levitation system shown in Eq. (8), the periodic solutions were found using the IHB method. The IHB method was proposed by Lau and Cheung [26] and it has been widely used to solve various nonlinear vibration problems. This method combines the incremental method used in numerical calculations and the harmonic balance method. It has been used successfully in the study of strongly nonlinear applications [27-33].

Letting $\tau = 2\pi ft = \omega t$, $s_p = s(\tau - \omega t_p)$, and $s'_d = s'(\tau - \omega t_d)$, Eq.(8) could be written as

$$\begin{aligned} &\omega^2 m \cdot s'' + \mu_{11} \cdot s_p + \mu_{12} \cdot s + \omega \mu_{21} \cdot s'_d + \mu_{31} \cdot s_p^2 + \mu_{32} \cdot s s_p + \mu_{33} \cdot s^2 \\ &+ \omega \mu_{41} \cdot s_p s'_d + \omega \mu_{42} \cdot s s'_d + \omega^2 \mu_{51} \cdot s'^2_d = H \sin \tau \end{aligned} \quad (9)$$

Letting s_0 and ω_0 denote a certain state in the vibration process, the critical state could be expressed in incremental form, as follows:

$$\begin{aligned} s &= s_0 + \Delta s \\ s_p &= s_{0p} + \Delta s_p \end{aligned} \quad (10)$$

$$\begin{aligned} s'_d &= s'_{0d} + \Delta s'_d \\ H &= H_0 + \Delta H \end{aligned} \quad (11)$$

$$\omega = \omega_0 + \Delta \omega \quad (12)$$

By substituting the above three equations into Eq.(9) and omitting higher-order terms, we obtained the following:

$$\begin{aligned} &\omega_0^2 m \cdot \Delta s'' + \mu_{11} \cdot \Delta s_p + \mu_{12} \cdot \Delta s + \omega_0 \mu_{21} \cdot \Delta s'_d + 2\mu_{31} s_{0p} \cdot \Delta s_p \\ &+ (\mu_{32} s_{0p} \cdot \Delta s + \mu_{32} s_0 \cdot \Delta s_p) + 2\mu_{33} s_0 \cdot \Delta s + (\omega_0 \mu_{41} s'_{0d} \cdot \Delta s_p + \omega_0 \mu_{41} s_{0p} \cdot \Delta s'_d) \\ &+ (\omega_0 \mu_{42} s'_{0d} \cdot \Delta s + \omega_0 \mu_{42} s_0 \cdot \Delta s'_d) + 2\omega_0^2 \mu_{51} s'_{0d} \cdot \Delta s'_d = \end{aligned} \quad (13)$$

$$\begin{aligned} &R - \left[2\omega_0 m s_0'' + \mu_{21} \cdot s'_{0d} + \mu_{41} \cdot s_{0p} s'_{0d} + \mu_{42} \cdot s_0 s'_{0d} + 2\omega_0 \mu_{51} \cdot s'^2_{0d} \right] \Delta \omega \\ &+ \Delta H \sin \tau \end{aligned}$$

$$\begin{aligned} R &= H_0 \sin \tau - \omega_0^2 m \cdot s_0'' - \mu_{11} \cdot s_{0p} - \mu_{12} \cdot s_0 - \omega_0 \mu_{21} \cdot s'_{0d} - \mu_{31} \cdot s_{0p}^2 - \mu_{32} \cdot s_0 s_{0p} \\ &- \mu_{33} \cdot s_0^2 - \omega_0 \mu_{41} \cdot s_{0p} s'_{0d} - \omega_0 \mu_{42} \cdot s_0 s'_{0d} - \omega_0^2 \mu_{51} \cdot s'^2_{0d} \end{aligned} \quad (14)$$

When s_0 , ω_0 , and H_0 were the exact solution of the equation; then $R=0$.

The periodic steady-state solution was expressed as follows:

$$\begin{aligned} s_0(\tau) &= a_0 + \sum_{k=1}^{N_c} a_k \cos k\tau + \sum_{k=1}^{N_s} b_k \sin k\tau = \mathbf{CA} \\ \Delta s(\tau) &= \Delta a_0 + \sum_{k=1}^{N_c} \Delta a_k \cos k\tau + \sum_{k=1}^{N_s} \Delta b_k \sin k\tau = \mathbf{C}\Delta\mathbf{A} \end{aligned} \quad (15)$$

Where

$$\begin{aligned}
\mathbf{C} &= [1, \cos \tau, \cos 2\tau, \dots, \cos N_c \tau, \sin \tau, \sin 2\tau, \dots, \sin N_s \tau] \\
\mathbf{A} &= [a_0, a_1, a_2, \dots, a_{N_c}, b_1, b_2, \dots, b_{N_s}]^T \\
\Delta \mathbf{A} &= [\Delta a_0, \Delta a_1, \Delta a_2, \dots, \Delta a_{N_c}, \Delta b_1, \Delta b_2, \dots, \Delta b_{N_s}]^T
\end{aligned} \tag{16}$$

Based on Eq.(15), the harmonic expansion of s_p and s'_d were as follows:

$$s_{0p} = a_0 + \sum_{k=1}^{N_c} a_k \cos(k\tau - k\omega t_p) + \sum_{k=1}^{N_s} b_k \sin(k\tau - k\omega t_p) \tag{17}$$

$$\Delta s_p = \Delta a_0 + \sum_{k=1}^{N_c} \Delta a_k \cos(k\tau - k\omega t_p) + \sum_{k=1}^{N_s} \Delta b_k \sin(k\tau - k\omega t_p)$$

$$s'_{0d} = \sum_{k=1}^{N_c} [-a_k k \sin(k\tau - k\omega t_d)] + \sum_{k=1}^{N_s} b_k k \cos(k\tau - k\omega t_d) \tag{18}$$

$$\Delta s'_d = \sum_{k=1}^{N_c} [-\Delta a_k k \sin(k\tau - k\omega t_d)] + \sum_{k=1}^{N_s} \Delta b_k k \cos(k\tau - k\omega t_d)$$

Letting $N_c = N_s = N$, Eq.(17) and (18) could be written in the following form:

$$\begin{aligned}
s_{0p} &= \mathbf{C} \mathbf{\Gamma}_p \mathbf{A}, \Delta s_p = \mathbf{C} \mathbf{\Gamma}_p \Delta \mathbf{A} \\
s'_{0d} &= \mathbf{C}' \mathbf{\Gamma}_d \mathbf{A}, \Delta s'_d = \mathbf{C}' \mathbf{\Gamma}_d \Delta \mathbf{A}
\end{aligned} \tag{19}$$

As shown in Eq.(19), we called $\mathbf{\Gamma}_p$ and $\mathbf{\Gamma}_d$ explicit time-

delay action matrices. They were expressed as follows:

$$\mathbf{\Gamma}_p = \begin{bmatrix} 1 & 0 & 0 & \dots & 0 & 0 & 0 & \dots & 0 \\ 0 & \cos(\omega t_p) & 0 & \dots & 0 & -\sin(\omega t_p) & 0 & \dots & 0 \\ 0 & 0 & \cos(2\omega t_p) & \dots & 0 & 0 & -\sin(2\omega t_p) & \dots & 0 \\ \vdots & \vdots & \vdots & \ddots & \vdots & \vdots & \vdots & \ddots & \vdots \\ 0 & 0 & 0 & \dots & \cos(N\omega t_p) & 0 & 0 & \dots & -\sin(N\omega t_p) \\ 0 & \sin(\omega t_p) & 0 & \dots & 0 & \cos(\omega t_p) & 0 & \dots & 0 \\ 0 & 0 & \sin(2\omega t_p) & \dots & 0 & 0 & \cos(2\omega t_p) & \dots & 0 \\ \vdots & \vdots & \vdots & \ddots & \vdots & \vdots & \vdots & \ddots & \vdots \\ 0 & 0 & 0 & \dots & \sin(N\omega t_p) & 0 & 0 & \dots & \cos(N\omega t_p) \end{bmatrix},$$

$$\mathbf{\Gamma}_d = \begin{bmatrix} 1 & 0 & 0 & \cdots & 0 & 0 & 0 & \cdots & 0 \\ 0 & \cos(\omega t_d) & 0 & \cdots & 0 & -\sin(\omega t_d) & 0 & \cdots & 0 \\ 0 & 0 & \cos(2\omega t_d) & \cdots & 0 & 0 & -\sin(2\omega t_d) & \cdots & 0 \\ \vdots & \vdots & \vdots & \ddots & \vdots & \vdots & \vdots & \ddots & \vdots \\ 0 & 0 & 0 & \cdots & \cos(N\omega t_d) & 0 & 0 & \cdots & -\sin(N\omega t_d) \\ 0 & \sin(\omega t_d) & 0 & \cdots & 0 & \cos(\omega t_d) & 0 & \cdots & 0 \\ 0 & 0 & \sin(2\omega t_d) & \cdots & 0 & 0 & \cos(2\omega t_d) & \cdots & 0 \\ \vdots & \vdots & \vdots & \ddots & \vdots & \vdots & \vdots & \ddots & \vdots \\ 0 & 0 & 0 & \cdots & \sin(N\omega t_d) & 0 & 0 & \cdots & \cos(N\omega t_d) \end{bmatrix}.$$

It was found that the time-

delay action matrices $\mathbf{\Gamma}_p$ and $\mathbf{\Gamma}_d$ were periodic functions of t_p and t_d , respectively. Their periods were $2\pi/\omega$ or $1/f$. Hence, we deduced that their impact on the maglev system was also periodic. Importantly, the solution would vary periodically with the changing of the time delay.

After substituting Eqs. (15) and (19) into Eq. (13)

and then applying the Galerkin process, we obtained a set of algebraic equations with the unknowns ΔA , $\Delta\omega$, and ΔH , which could be expressed as follows:

$$\mathbf{K}_{mc} \Delta A = \mathbf{R} + \mathbf{R}_{mc} \Delta\omega + \mathbf{R}_h \Delta H, \quad (20)$$

$$\begin{aligned} \mathbf{K}_{mc} = & \omega_0^2 \mathbf{M} + \mathbf{K}_{11} + \mathbf{K}_{12} + \omega_0 \mathbf{C}_{21} + 2\mathbf{K}_{31} \\ & + \mathbf{K}_{32}^1 + \mathbf{K}_{32}^2 + 2\mathbf{K}_{33} + \omega_0 \mathbf{C}_{41}^1 + \omega_0 \mathbf{C}_{41}^2, \\ & + \omega_0 \mathbf{C}_{42}^1 + \omega_0 \mathbf{C}_{42}^2 + 2\omega_0^2 \mathbf{C}_{51} \end{aligned} \quad (21)$$

$$\begin{aligned} \mathbf{R} = & \mathbf{H} - \left[\omega_0^2 \mathbf{M} + \mathbf{K}_{11} + \mathbf{K}_{12} + \omega_0 \mathbf{C}_{21} + \mathbf{K}_{31} \right. \\ & \left. + \mathbf{K}_{32}^1 + \mathbf{K}_{33} + \omega_0 \mathbf{C}_{41}^2 + \omega_0 \mathbf{C}_{42}^2 + \omega_0^2 \mathbf{C}_{51} \right] \mathbf{A}, \end{aligned} \quad (22)$$

$$\mathbf{R}_{mc} = - \left[2\omega_0 \mathbf{M} + \mathbf{C}_{21} + \mathbf{C}_{41}^2 + \mathbf{C}_{42}^2 + 2\omega_0 \mathbf{C}_{51} \right] \mathbf{A}, \quad (23)$$

where

$$\begin{aligned}
\mathbf{M} &= \int_0^{2\pi} \mathbf{C}^T m \mathbf{C} d\tau, \\
\mathbf{K}_{11} &= \int_0^{2\pi} \mathbf{C}^T \mu_{11} \mathbf{C} \Gamma_p d\tau, \mathbf{K}_{12} = \int_0^{2\pi} \mathbf{C}^T \mu_{12} \mathbf{C} d\tau \\
\mathbf{C}_{21} &= \int_0^{2\pi} \mathbf{C}^T \mu_{21} \mathbf{C}' \Gamma_d d\tau \\
\mathbf{K}_{31} &= \int_0^{2\pi} \mathbf{C}^T \mu_{31} s_{0p} \mathbf{C} \Gamma_p d\tau, \mathbf{K}_{32}^1 = \int_0^{2\pi} \mathbf{C}^T \mu_{32} s_{0p} \mathbf{C} d\tau \\
\mathbf{K}_{32}^2 &= \int_0^{2\pi} \mathbf{C}^T \mu_{32} s_{0d} \mathbf{C} \Gamma_p d\tau, \mathbf{K}_{33} = \int_0^{2\pi} \mathbf{C}^T \mu_{33} s_{0d} \mathbf{C} d\tau \\
\mathbf{C}_{41}^1 &= \int_0^{2\pi} \mathbf{C}^T \mu_{41} s_{0d}' \mathbf{C} \Gamma_p d\tau, \mathbf{C}_{41}^2 = \int_0^{2\pi} \mathbf{C}^T \mu_{41} s_{0p} \mathbf{C}' \Gamma_d d\tau \\
\mathbf{C}_{42}^1 &= \int_0^{2\pi} \mathbf{C}^T \mu_{42} s_{0d}' \mathbf{C} d\tau, \mathbf{C}_{42}^2 = \int_0^{2\pi} \mathbf{C}^T \mu_{42} s_{0d} \mathbf{C}' \Gamma_d d\tau \\
\mathbf{C}_{51} &= \int_0^{2\pi} \mathbf{C}^T \mu_{51} s_{0d}' \mathbf{C}' \Gamma_d d\tau \\
\mathbf{H} &= \int_0^{2\pi} \mathbf{C}^T H_0 \cos \tau d\tau, \mathbf{R}_h = \int_0^{2\pi} \mathbf{C}^T \cos \tau d\tau
\end{aligned} \tag{24}$$

If we were only concerned with the frequency—
amplitude response curve at a certain aerodynamic amplitude, then \mathbf{H} had a fixed value and $\Delta H = 0$. Thus, Eq. (20) became

$$\mathbf{K}_{mc} \Delta \mathbf{A} = \mathbf{R} + \mathbf{R}_{mc} \Delta \omega \tag{25}$$

Equation (25)

represents a set of linear equations. Its number of unknowns was greater than the number of equations by one, so in the solution process, one of the increments was selected as a parameter. We could choose the amplitude a of a certain harmonic or the excitation frequency as the control increment. The Newton-Raphson iterative method was adopted to calculate the solution when the frequency ω or one component of the amplitude \mathbf{A} was given. The criterion for stopping an iteration was that the corrective vector \mathbf{R}_w was small enough. To efficiently calculate the amplitude—
frequency response curve, the sampling arc length increment method used in this research automatically tracked the response curve. Readers are referred to the work of Cheung [34] for the associated theory of the arc length increment method.

4 Stability

We let s_0 be the obtained steady-

state periodic solution and let Δs be a perturbation. By substituting $s = s_0 + \Delta s$ into Eq.(9)

and omitting the high-order small quantities, we obtained the perturbation equations:

$$\begin{aligned} & \omega_0^2 m \Delta s'' + \mu_{11} \cdot \Delta s_p + \mu_{12} \cdot \Delta s + \omega_0 \mu_{21} \cdot \Delta s_d' \\ & + \mu_{31} 2s_{0p} \cdot \Delta s_p + (\mu_{32} s_{0p} \cdot \Delta s + \mu_{32} s_0 \cdot \Delta s_p) + 2\mu_{33} s_0 \cdot \Delta s \\ & + (\omega_0 \mu_{41} s_{0d}' \cdot \Delta s_p + \omega_0 \mu_{41} s_{0p} \cdot \Delta s_d') \\ & + (\omega_0 \mu_{42} s_{0d}' \cdot \Delta s + \omega_0 \mu_{42} s_0 \cdot \Delta s_d') \\ & + 2\omega_0^2 \mu_{51} s_{0d}' \cdot \Delta s_d' = 0 \end{aligned} \quad (26)$$

The stability of the solution of the original equation corresponded to the stability of the solution of the ordinary differential equations (Eq.(26)) with periodic coefficients and a time delay.

For a time-

delayed system containing periodic coefficients, we first converted the differential equation with a time delay to a differential equation without a time delay using the finite difference continuous time approximation method, after which we studied the stability of the time-delayed system with periodic coefficients using Floquet theory.

Letting

$$\mathbf{q} = [q_1, q_2]^T = [\Delta s', \Delta s]^T \quad (27)$$

Eq.(26) could be written in matrix form as follows:

$$\begin{aligned} \dot{\mathbf{q}} &= \mathbf{f}[\mathbf{q}(\tau), \mathbf{q}(\tau - \omega t_p), \mathbf{q}(\tau - \omega t_d)] = \mathbf{G}\mathbf{q}(\tau) + \mathbf{G}_p \mathbf{q}(\tau - \omega t_p) + \mathbf{G}_d \mathbf{q}(\tau - \omega t_d) \\ \mathbf{G} &= \begin{bmatrix} 0 & -\frac{1}{\omega_0^2 m} (\mu_{12} + \mu_{32} s_{0p} + 2\mu_{33} s_0 + \omega_0 \mu_{42} s_{0d}') \\ 1 & 0 \end{bmatrix} \\ \mathbf{G}_p &= \begin{bmatrix} 0 & -\frac{1}{\omega_0^2 m} (\mu_{11} + 2\mu_{31} s_{0p} + \mu_{32} s_0 + \omega_0 \mu_{41} s_{0d}') \\ 0 & 0 \end{bmatrix} \\ \mathbf{G}_d &= \begin{bmatrix} -\frac{1}{\omega_0^2 m} (\omega_0 \mu_{21} + \omega_0 \mu_{41} s_{0p} + \omega_0 \mu_{42} s_0 + 2\omega_0^2 \mu_{51} s_{0d}') & 0 \\ 0 & 0 \end{bmatrix} \end{aligned} \quad (28)$$

The state variables were expressed in terms of $\mathbf{q}(\tau)$, $\mathbf{q}(\tau - \tau_1)$, and $\mathbf{q}(\tau - \tau_2)$, (where $0 < \tau_1 \leq \omega t_p$, $0 < \tau_2 \leq \omega t_d$) had infinite dimensions. The state variables with a time delay $\mathbf{q}(\tau - \tau_1)$, $0 < \tau_1 \leq \omega t_p$, $\mathbf{q}(\tau - \tau_2)$, $0 < \tau_2 \leq \omega t_d$ could be discretized. Assuming that N_p and N_d are integers, we obtained $\Delta \tau_p = \omega t_p / N_p$ and $\Delta \tau_d = \omega t_d / N_d$. The derivatives of $\dot{\mathbf{q}}(\tau - i \cdot \Delta \tau_p)$ and $\dot{\mathbf{q}}(\tau - i \cdot \Delta \tau_d)$ were approximated with the following differences:

$$\begin{aligned}\dot{\mathbf{q}}(\tau - i \cdot \Delta \tau_p) &= \frac{1}{\Delta \tau_p} [\mathbf{q}(\tau - (i-1) \cdot \Delta \tau_p) - \mathbf{q}(\tau - i \cdot \Delta \tau_p)] \\ \dot{\mathbf{q}}(\tau - i \cdot \Delta \tau_d) &= \frac{1}{\Delta \tau_d} [\mathbf{q}(\tau - (i-1) \cdot \Delta \tau_d) - \mathbf{q}(\tau - i \cdot \Delta \tau_d)]\end{aligned}\quad (29)$$

The following finite dimensional state variable was defined:

$$\begin{aligned}\mathbf{p}(\tau) &= [\mathbf{q}(\tau), \mathbf{q}(\tau - \Delta \tau_p), \mathbf{q}(\tau - 2\Delta \tau_p), \dots, \mathbf{q}(\tau - N_p \Delta \tau_p), \\ &\quad \mathbf{q}(\tau - \Delta \tau_d), \mathbf{q}(\tau - 2\Delta \tau_d), \dots, \mathbf{q}(\tau - N_d \Delta \tau_d)]^T \\ &= [\mathbf{p}_1(\tau), \mathbf{p}_2(\tau), \mathbf{p}_3(\tau), \dots, \mathbf{p}_{N_p+N_d+1}(\tau)]^T\end{aligned}\quad (30)$$

The following system equation could be obtained based on the expansion state variables shown in Eq.

(30):

$$\dot{\mathbf{p}}(\tau) = \begin{bmatrix} f[\mathbf{q}(\tau), \mathbf{q}(\tau - \tau_p), \mathbf{q}(\tau - \tau_d)] \\ \frac{1}{\Delta \tau_p} [\mathbf{p}_1(\tau) - \mathbf{p}_2(\tau)] \\ \vdots \\ \frac{1}{\Delta \tau_p} [\mathbf{p}_{N_p}(\tau) - \mathbf{p}_{N_p+1}(\tau)] \\ \frac{1}{\Delta \tau_d} [\mathbf{p}_1(\tau) - \mathbf{p}_{N_p+2}(\tau)] \\ \frac{1}{\Delta \tau_d} [\mathbf{p}_{N_p+2}(\tau) - \mathbf{p}_{N_p+3}(\tau)] \\ \vdots \\ \frac{1}{\Delta \tau_d} [\mathbf{p}_{N_p+N_d}(\tau) - \mathbf{p}_{N_p+N_d+1}(\tau)] \end{bmatrix} = \boldsymbol{\psi} \cdot \mathbf{p}(\tau)\quad (31)$$

where

$$\Psi = \begin{bmatrix} \mathbf{G} & 0 & \dots & 0 & \mathbf{G}_p & \dots & \dots & 0 & \mathbf{G}_d \\ \frac{1}{\Delta\tau_p} \mathbf{I} & \frac{1}{\Delta\tau_p} \mathbf{I} & & & & & & & \\ & & \ddots & & & & & & \\ & & & \frac{1}{\Delta\tau_p} \mathbf{I} & -\frac{1}{\Delta\tau_p} \mathbf{I} & & & & \\ \frac{1}{\Delta\tau_d} \mathbf{I} & & & & -\frac{1}{\Delta\tau_d} \mathbf{I} & & & & \\ & & & & \frac{1}{\Delta\tau_d} \mathbf{I} & -\frac{1}{\Delta\tau_d} \mathbf{I} & & & \\ & & & & & \ddots & & & \\ & & & & & & \frac{1}{\Delta\tau_d} \mathbf{I} & -\frac{1}{\Delta\tau_d} \mathbf{I} & \end{bmatrix} \quad (32)$$

In the above Eq.(32), $\mathbf{I} = \text{diag}(1, 1)$. The stability of the control equation (Eq.(26)) could be assessed using the stability of Eq.(31).

Since s_0, s_{0p} , and $ds_{0d}/d\tau$ were periodic functions with a period of $T = 2\pi/\omega$, Ψ was also a periodic function with the same period as s_0 . We assumed that the matrix Φ was the basic solution matrix of Eq.(32) and that it satisfied

$$\begin{aligned} \dot{\Phi}(\tau) &= \Psi(\tau) \Phi(\tau) \\ \dot{\Phi}(\tau + T) &= \Psi(\tau) \Phi(\tau + T) \\ \Phi(\tau + T) &= \mathbf{C} \Phi(\tau) \end{aligned} \quad (33)$$

\mathbf{C} is the transfer matrix. According to Floquet theory, the stability of a system depends on the eigenvalues of the matrix \mathbf{C} . If the modulus of all the eigenvalues of \mathbf{C} are less than 1, then the motion of the system is bounded and the solution is stable; otherwise, the motion is unbounded and the solution is unstable.

Choosing an initial condition of $\Phi(0) = \mathbf{I}$, the basic solution of Eq.(32) was solved numerically, and we obtained the following:

$$\mathbf{C} = \Phi(T) \quad (34)$$

According to the method given by Friedmann [35], the transition matrix could be obtained with the fourth-order Runge–Kutta numerical integration method.

5 Analysis of Numerical Example

Based on the aforementioned theory, we wrote a program for the periodic solution and stability analysis. We examined an electromagnet module for an actual high-speed maglev train and we selected parameters based on 1/8 of a vehicle. Table 1 shows the parameters selected.

Table 1 Electromagnet parameters

m (kg)	μ_0 (H/m)	δ_0 (m)	N_m	R (Ω)	A_m (m ²)
6300	$4\pi \times 10^{-7}$	0.01	290	0.61	0.622

The aerodynamic amplitude was $A_0 = 25000$ N and the reference area of the vehicle was 11.86 m². Since the parameters were selected based on 1/8 of a vehicle, the steady aerodynamic lift needed to be 1/8 of the aerodynamic lift that the entire vehicle was subjected to, $F_{L_0} = 0.5 C_L \rho A_v v^2 / 8$.

5.1 Procedure verification

To ensure the reliability of the analysis program, we calculated the periodic solutions considering the time delays in the position feedback and compared them with the stable periodic solution calculated using the Runge–Kutta direct integration method.

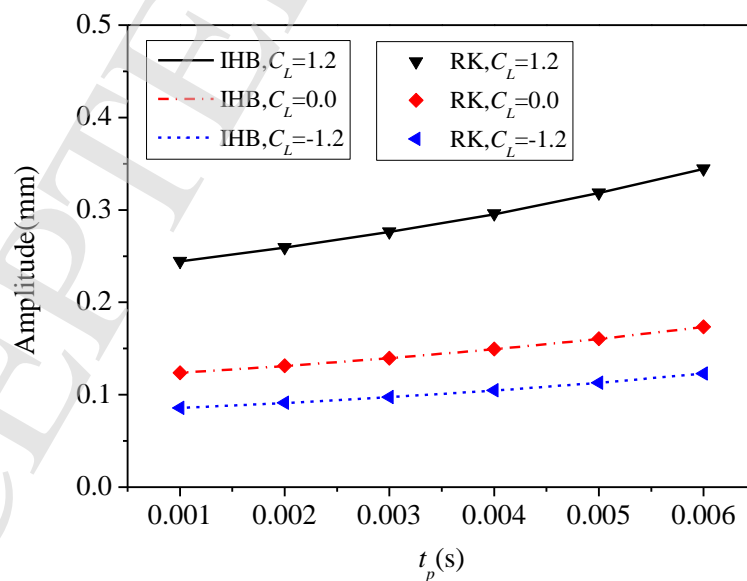


Figure 2 Comparison of the calculated results using the IHB method and the Runge–Kutta method

Figure 2 shows the vibration amplitudes of periodic solutions with different time delays for the position feedback t_p .

The other parameters were $k_p=2000$, $k_d=20$, and $f=10$ Hz. The amplitudes of the periodic solutions obtained by the two methods were equal, which verified the correctness of the analysis program.

Based on the verified analysis program, we investigated the nonlinear vibrations of the maglev system under the action of aerodynamic lift for three time-delay scenarios. The three scenarios considered only the time delay of the position feedback t_p , only the time delay of the velocity feedback t_d , and both the time delay of the position feedback t_p and the time delay of the velocity feedback t_d . The steady aerodynamic lift had an important effect on the stability of the maglev train. For each time-delay scenario, we calculated the response and stability of the maglev system for $C_L=1.2$ (vertically upward steady lift), $C_L=0.0$ (zero steady lift), and $C_L=-1.2$ (vertically downward steady lift).

5.2 Time delay of position feedback

In this subsection, we present the analysis results for the scenario in which only the time delay of the position feedback t_p was considered. For this scenario, we set $k_p=2000$ and $k_d=20$. Figure 3 presents the relationship curves between the periodic vibration amplitude and the time delay of the position feedback for three steady lift conditions. The analysis results showed that the vibration amplitude was a maximum when the steady aerodynamic lift coefficient was $C_L=1.2$, followed by that at $C_L=0$, and it was a minimum at $C_L=-1.2$. This showed that when the steady aerodynamic lift was vertically upward, the vibration amplitude of the system excited by unsteady aerodynamic lift would be greater. In addition, the figures show that when the excitation frequency was 15 Hz, the amplitude was a maximum.

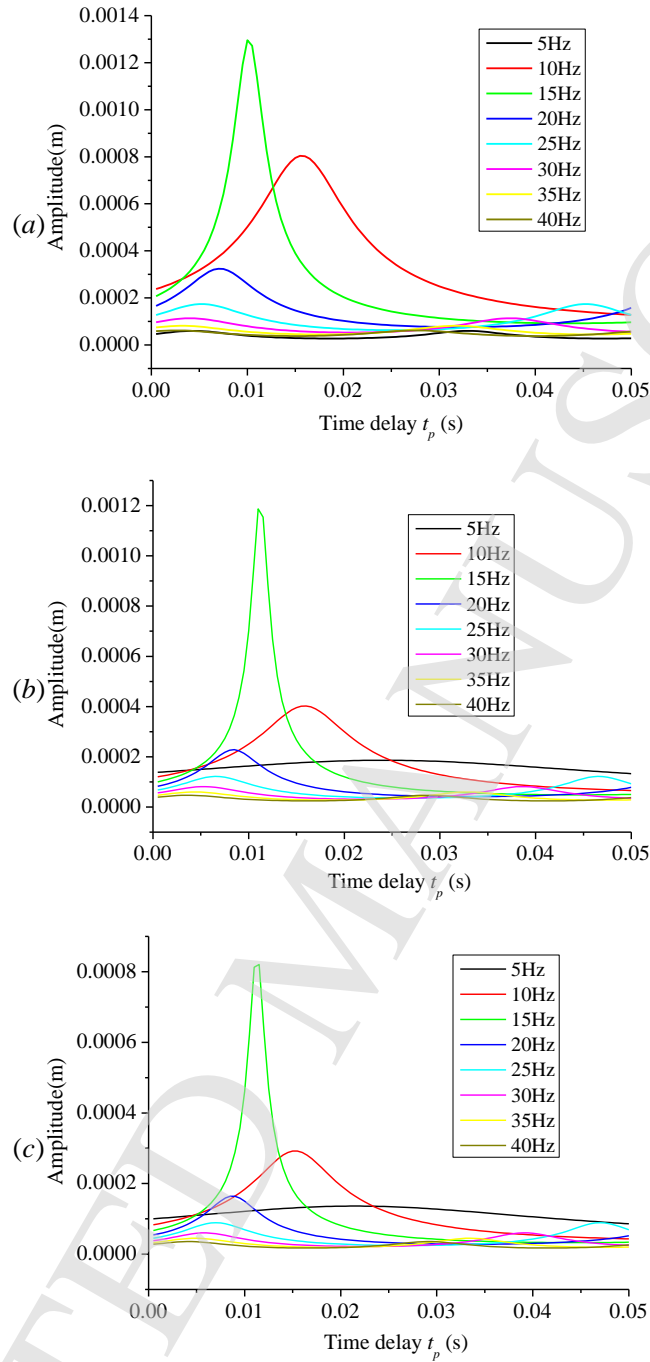


Figure 3 Relationship between periodic vibration amplitude and position time delay: (a) $C_L = 1.2$; (b) $C_L = 0$; (c) $C_L = -1.2$

It is worth noting that the time-

delay action matrix was periodic in terms of t_d with a period of $T = 1/f_j$, just as shown in Eq. (19). Thus, the periodic solution had to exhibit periodic variations with respect to the time delay. The results shown in Fi

Figure 3 confirmed this deduction. Figure 3 shows that for a low-frequency excitation, the period of the amplitude change with the time delay was long. For the time delay of the position feedback in the 0–0.05 s range, the amplitude increased monotonically. At high excitation frequencies, with the time delay of the position feedback in the 0–0.05 s range, the amplitude variation with the time delay of the position feedback appeared periodically.

From the stability analysis of the periodic solution, we obtained the critical time delay of the system instability. Table 2 shows the critical time delay of the position feedback for $f=10\text{Hz}$ and 20Hz . The results showed that the excitation frequency of the unsteady lift had no effect on the critical time delay. The critical time delay was small at $C_L=1.2$ and greater at $C_L=0$ and -1.2 , but the overall difference was small.

Table 2 Comparison of critical time delays for different steady aerodynamic lift coefficients

	$f=10\text{Hz}$	$f=20\text{Hz}$
$C_L=1.2$	0.01195s	0.01195s
$C_L=0$	0.01230s	0.0123s
$C_L=-1.2$	0.01225s	0.01225s

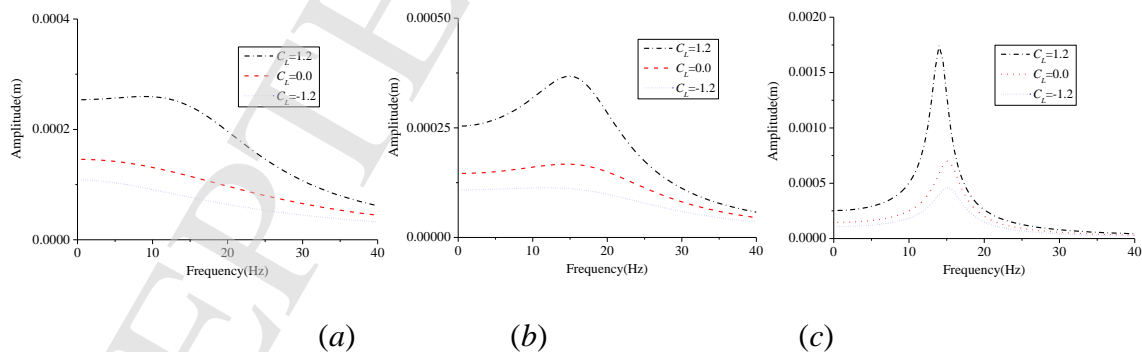


Figure 4 Amplitude-frequency response curves for different time delays of the position feedback: (a) $t_p=0.002\text{s}$, stable; (b) $t_p=0.005\text{s}$, stable; (c) $t_p=0.01\text{s}$, stable

Figure 4 shows the amplitude–

frequency response curve for three different time delays of the position feedback. The results show more clearly that the maximum amplitudes were all in the vicinity of 15 Hz. Compared to the case without steady aerodynamic lift, the amplitude was greater when the steady aerodynamic lift was directed vertically upward and lesser when the steady aerodynamic lift was directed vertically downward.

Figure 5 and Figure 6 display the dependence of the critical time delay of the position feedback on the position feedback gain k_p and the velocity feedback gain k_d , respectively. The results showed that when k_p increased, the critical time delay of the position feedback decreased. When k_d increased, the critical time delay of the position feedback increased. In addition, the critical time delays of the position feedback corresponding to $C_L = 1.2, 0$, and -1.2 were similar.

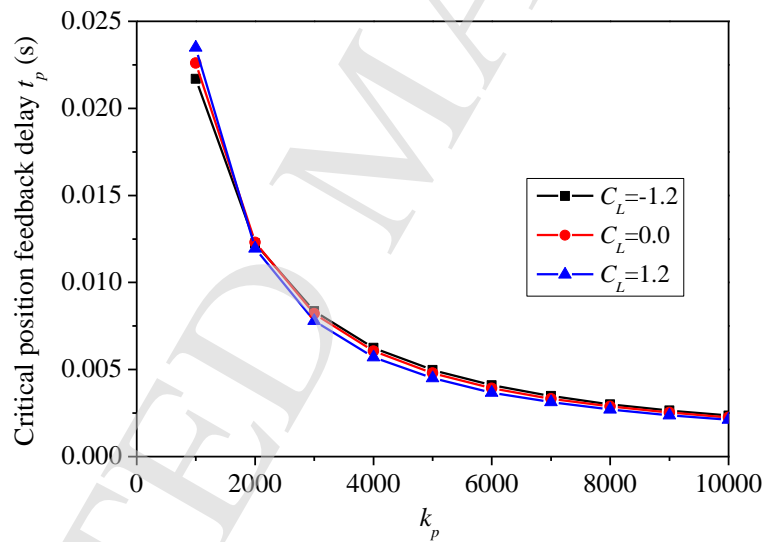


Figure 5 Relationship between the critical time delay of the position feedback and the position feedback gain ($k_d = 20, f = 10 \text{ Hz}$)

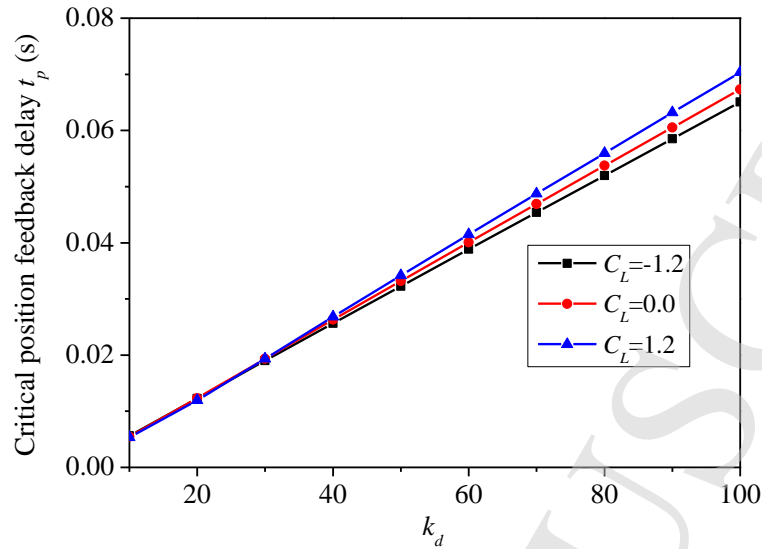


Figure 6 Relationship curves for the critical time delay of the position feedback and the velocity feedback gain ($k_p=2000, f=10\text{Hz}$)

5.3 Time delay of velocity feedback

This sub-

section shows the nonlinear response of the maglev system under the action of aerodynamic lift for the scenario in which only the time delay of the velocity feedback t_d was considered. In the analysis described in this section, we chose the following values: $k_p=2000, k_d=20, H=25000\text{N}$.

Figure 7 shows the relationship curves for the amplitude of the periodic vibration and the time delay t_d under three steady aerodynamic lift conditions: $C_L=1.2, 0$, and -1.2 . Similarly, when the steady aerodynamic lift was vertically upward, the response amplitude of the system was greater. Equation (19) also shows that the effect of t_d on the system was periodic, with a period of $T=1/f$, which is also reflected in Figure 7.

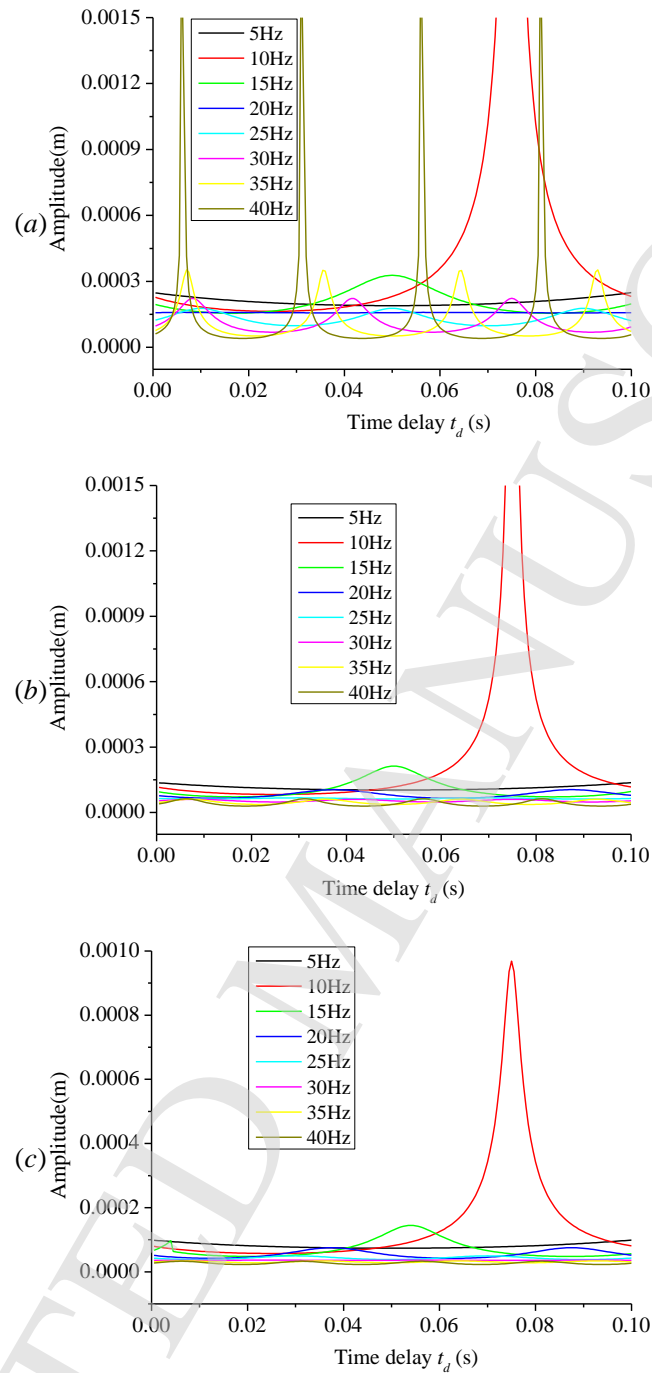


Figure 7 Relationship curves for the periodic vibration amplitude and time delay of the position feedback: (a) $C_L = 1.2$; (b) $C_L = 0$; (c) $C_L = -1.2$

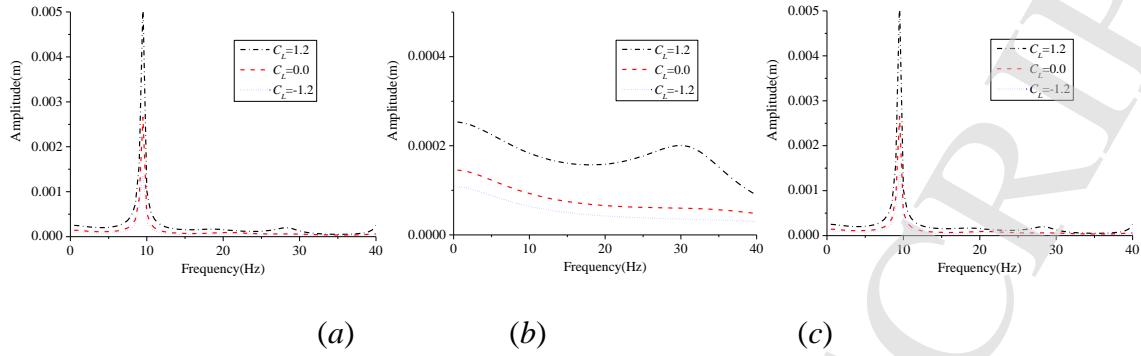


Figure 8 Amplitude–

frequency response curve for different time delays of the velocity feedback: (a) $t_p=0.002$ s, stable; (b) $t_p=0.01$ s, unstable; (c) $t_p=0.08$ s, unstable

In addition, when considering only the time delay of the position feedback, the maximum amplitude occurred at a frequency of 15 Hz, and when considering only the time delay of the velocity feedback, the frequency was about 10 Hz, as shown in Figure 8.

Figure 9 and Figure 10 show the dependence of the critical time delay of the velocity feedback on the position feedback gain k_p and the velocity feedback gain k_d , respectively. The results showed that the critical time delay of the velocity feedback decreased as k_p and k_d increased. When compared to the case of $C_L=0$, the critical time delay of the velocity feedback was greater when the steady aerodynamic lift was in the upward direction ($C_L=1.2$), and the critical time delay of the velocity feedback was smaller when the steady aerodynamic lift was vertically downward ($C_L=-1.2$).

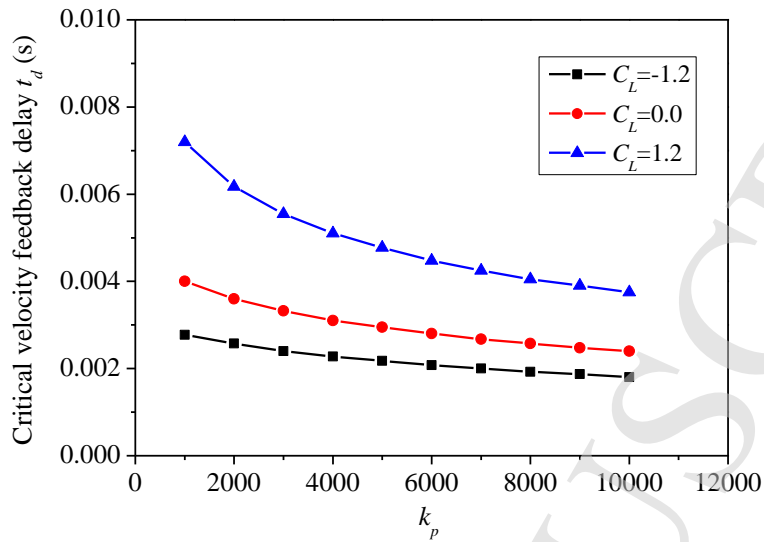


Figure 9 Relationship between the critical time delay of the velocity feedback and the position feedback gain k_p ($k_d=20, f=10\text{Hz}$)

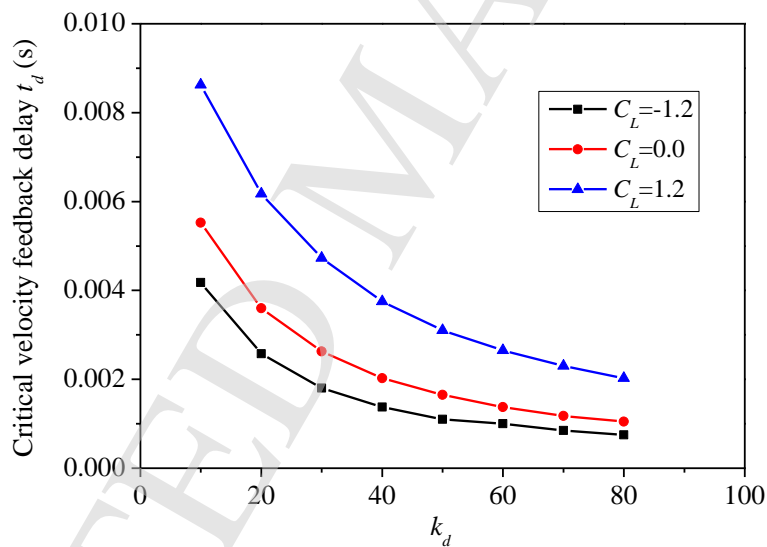


Figure 10 Relationship between the critical time delay of the velocity feedback and the velocity feedback gain k_d ($k_p=2000, f=10\text{Hz}$)

5.4 Dual time delay in position and velocity feedback

To address the case of a dual time delay in the position and velocity feedback control loop, we analyzed the stability of the periodic solution of the maglev system under the action of aerodynamic lift and obtained the stability boundary for the time delay, as shown in Figure 11. The figure shows the time-

delay stability boundary curves when the steady aerodynamic lift coefficient was equal to 1.2, 0, and -1.2. When the time delay of the position feedback and the time delay of the velocity feedback were located on the lower left side of a curve, the response of the maglev system under the aerodynamic lift was stable. When the time delay was located on the upper right-hand side of a curve, the response was unstable.

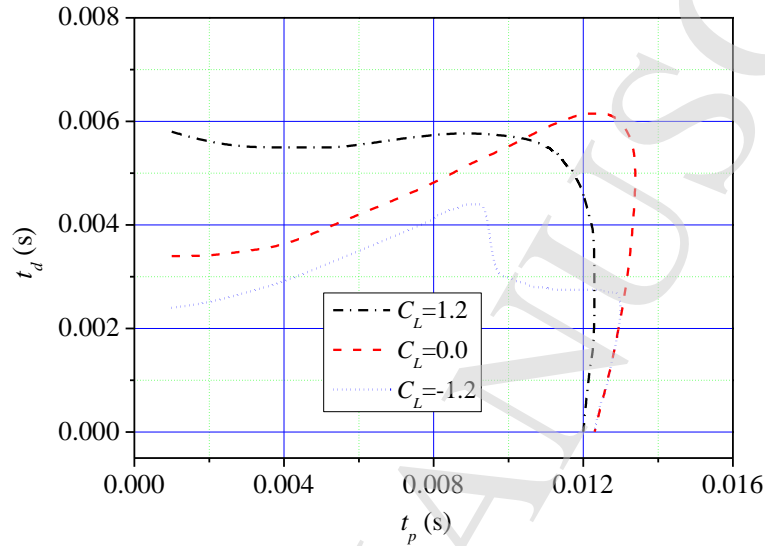


Figure 11 Stability boundary with simultaneous time delays of position feedback and velocity feedback ($k_p=2000, k_d=20, H=25000\text{N}, f=10\text{Hz}$)

6 Conclusion

In this study, we established a nonlinear model for a maglev system under the combined effect of steady and unsteady aerodynamic lift and time-delayed feedback control. The nonlinear periodic solution of the system was calculated using the IHB method, and the stability of the periodic solution was assessed using the continuous time approximation method and the multi-variable Floquet theory to obtain the critical time delay. Based on a 1/8 maglev vehicle, we conducted an analysis and obtained the relationship between the periodic vibration amplitude of the maglev system with aerodynamic lift plus a time delay and the frequency of the aerodynamic lift. We also obtained the relationship curve for the critical time delay of the position feedback, the critical time delay of the velocity feedback, and the control gain parameter as we

llasthestabilityboundarywhenthe timedelaysofboththepositionfeedbackandthevelocityfeedback wereconsidered.

We arrived at the following main conclusions:

(1) Compared to the case where the steady aerodynamic lift was zero, the response vibration amplitude of the system increased if the steady aerodynamic lift was vertically upward and the response amplitude of the system will decrease if the aerodynamic lift was vertically downward.

(2) There were explicit time-delay action matrices. The action matrices revealed that the effect of the time delay on the response of the maglev system was periodic, with the period equal to $1/f$, where f is the fluctuation frequency of the unsteady aerodynamic lift. The numerical analysis confirmed this.

(3) The fluctuation frequency of the unsteady aerodynamic lift had no effect on the critical time delay of the system instability.

(4) When k_p increased, the critical time delay of the position feedback decreased. However, when k_d increased, the critical time delay of the position feedback increased. Nevertheless, the critical time delay of the velocity feedback decreased as k_p and k_d increased.

(5) Compared to the case where the steady aerodynamic lift was zero ($C_L=0$), the critical time delay of the velocity feedback increased if the steady aerodynamic lift was vertically upward ($C_L=1.2$), and the critical time delay of the velocity feedback decreased if the steady aerodynamic lift was downward ($C_L=-1.2$). However, for all three conditions of the steady aerodynamic lift, the differences in the critical time delay of the position feedback were small.

These findings and conclusions could be extended to an entire vehicle, which would be of helpful understanding the suspension characteristics of a maglev vehicle. For instance, the vibration amplitude under aerodynamic lift could guide the aerodynamic shape design of a maglev vehicle, so that the aerodynamic lift generated by the vehicle shape could avoid the area of large vibration amplitude. Another example is the relationship between the critical time delay and the feedback control gains, according

to which the control gain parameters could be selected to enable the vehicle system to have a high tolerance for time delay and to improve the control performance.

Acknowledgements

This project was supported by the National Key R&D Program of China (Grant 2016YFB1200602), the National Natural Science Foundation of China (Grants 51805522, 11672306, and 51490673), the Strategic Priority Research Program of the Chinese Academy of Sciences (Grant XDB22020100) and the Informatization Plan of the Chinese Academy of Sciences (Grant XXH13506-204).

REFERENCES

1. Wang Z L, Xu Y L, Li G Q, et al. Dynamic Analysis of a Coupled System of High-Speed Maglev Train and Curved Viaduct. *International Journal of Structural Stability and Dynamics*, 2018, 18(11): 1850143.
2. Wang D X, Li X Z, Wu Z Y. Dynamic Performance of the LMS Maglev Train–Track–Bridge System Under Uneven Settlement for Two Typical Bridges. *International Journal of Structural Stability and Dynamics*, 2020. DOI: 10.1142/S0219455421500061.
3. Luo C Y, Zhou D, Chen G, et al. Aerodynamic Effects as a Maglev Train Passes Through a Noise Barrier. *Flow Turbulence And Combustion*, 2020, 105(3): 761-785.
4. Zhou P, Zhang J Y, Li T, et al. Numerical study on wave phenomena produced by the super high-speed evacuated tube maglev train. *Journal of Wind Engineering and Industrial Aerodynamics*, 2019, 190: 61-70.
5. Gao D G, Ni F, Lin G B, et al. Aerodynamic analysis of pressure wave of high-speed maglev vehicle crossing: modeling and calculation. *Energies*, 2019, 12: 3770
6. Zhou P, Li T, Zhao C F, et al. Numerical study on the flow field characteristics of the new high-speed maglev train in open air. *Journal of Zhejiang University - SCIENCE A*

- (Applied Physics & Engineering), 2020, 21(5): 366-381.
7. Huang S, Li Z W, Yang M Z. Aerodynamics of high-speed maglev trains passing each other in open air. *Journal of Wind Engineering and Industrial Aerodynamics*, 2019, 188: 151-160.
 8. Kwon S D, Lee J S, Moon J W, et al. Dynamic interaction analysis of urban transit maglev vehicle and guideway suspension bridge subjected to gusty wind. *Engineering Structures*, 2008, 30(12): 3445-3456.
 9. Yau J D. Aerodynamic vibrations of a maglev vehicle running on flexible guideways under oncoming wind actions. *Journal of Sound and Vibration*, 2010, 329(10) 1743-1759.
 10. Wu J J, Shi X H. Numerical analyses of dynamic stability of maglev vehicles in crosswind field. *Journal of University (Natural Sciences)*, 2009, 45(2): 96-102. (in Chinese)
 11. Wu H, Zeng X H, Yu Y. Motion stability of high-speed maglev systems in consideration of aerodynamic effect: a study of a single magnetic suspension system. *Acta Mechanica Sinica*, 2017, 33(6): 1084-1094
 12. Wang H P. *Vehicle-Guideway Dynamic Interaction of the EMS Low Speed Maglev Vehicle*. Changsha: National University of Defense Technology, 2007 (in chinese)
 13. Xu J Q, Chen C, Gao D G, et al. Nonlinear dynamic analysis on maglev train system with flexible guideway and double time-delay feedback control. *Journal of Vibroengineering*, 2017, 19(8): 6346-6362.
 14. Li J H, Li J, Zhou D F, et al. Self-excited vibration problems of maglev vehicle-bridge interaction system. *Journal of Central South University*, 2014, 21(11): 4184-4192.
 15. Wang H P, Li J, Zhang K. Stability and Hopf bifurcation of the maglev system with delayed speed feedback control. *Acta Automatica Sinica*, 2007, 33(8): 829-834.

16. Wang H P, Li J, Zhang K. Non-resonant response, bifurcation and oscillation suppression of a non-autonomous system with delayed position feedback control. *Nonlinear Dynamics*, 2008, 51(3): 447-464.
17. Wang H P, Li J, Zhang K. Sup-resonant response of a non-autonomous maglev system with delayed acceleration feedback control. *IEEE Transactions on Magnetics*, 2008, 44(10): 2338-2350
18. Zhang L L, Campbell S A, Huang L H. Nonlinear analysis of a maglev system with time-delayed feedback control. *Physica D-Nonlinear Phenomena*, 2011, 240(21): 1761-1770.
19. Zhang L L, Huang L H, Zhang Z Z. Stability and Hopf bifurcation of the maglev system with delayed position and speed feedback control. *Nonlinear Dynamics*, 2009, 57(1-2): 197-207.
20. Zhang L L, Zhang Z Z, Huang L H. Double Hopf bifurcation of time-delayed feedback control for maglev system. *Nonlinear Dynamics*, 2012, 69(3): 961-967.
21. Zhang Z Z, Zhang L L. Hopf bifurcation of time-delayed feedback control for maglev system with flexible guideway. *Applied Mathematics & Computation*, 2013, 219(11): 6106-6112.
22. Zhang L L, Huang J H, Huang L H, et al. Stability and Bifurcation Analysis in a Maglev System with Multiple Delays. *International Journal of Bifurcation And Chaos*, 2015, 25(5): 1550074
23. Sun Y G, Chen C, Xu J Q, et al. Research on Coupled Vibration Mechanism of Vehicle-Rail System Considering the Effect of Track Elasticity on Time Delay. *IEEE Annual International Conference on Cyber Technology in Automation Control and Intelligent Systems*, 2019: 137-141.
24. Sun Y G, Xie S, Xu J Q, et al. A Robust Levitation Control of Maglev Vehicles Subject to

- Time Delay and Disturbances: Design and Hardware Experimentation. Applied Sciences-Basel, 2020, 10(3): 1179.
25. Yang YB, Yau J D, Urushadze S. Wave attenuation of a pre-tensioned wire with periodic spring supports subjected to a moving force, *International Journal of Structural Stability and Dynamics*, 2020, 20(11): 2071009.
26. Lau SL, Cheung YK. Amplitude incremental variational principle for nonlinear vibration of elastic systems. ASME, *Journal of Applied Mechanics*, 1981, 48: 959-964.
27. Mitra R K, Banik A K, Chatterjee S. Response of a harmonically forced dry friction damped system under time-delayed state feedback. *Journal of Computational and Nonlinear Dynamics*, 2018, 13: 031001.
28. Shen Y J, Wen S F, Li X H, et al. Dynamical analysis of fractional-order nonlinear oscillator by incremental harmonic balance method. *Nonlinear Dynamics*, 2016, 85(3): 1457–1467.
29. Liu Y B, Xing Y L, Law S S, et al. Internal resonance vibration induced by nonlinearity of primary suspension system in high-speed vehicle system. *Nonlinear Dynamics*, 2017, 88(4): 2947–2956.
30. Wang S, Hua L, Yang C, et al. Applications of incremental harmonic balance method combined with equivalent piecewise linearization on vibrations of nonlinear stiffness systems. *Journal of Sound and Vibration*, 2019, 441: 111–125.
31. Huang J L, Zhu W D. A new incremental harmonic balance method with two time scales for quasi-periodic motions of an axially moving beam with internal resonance under single-tone external excitation. *Journal of Vibration and Acoustics*, 2017, 139(2): 021010.
32. Li Y L, Chen S Y. Periodic solution and bifurcation of a suspension vibration system by incremental harmonic balance and continuation method. *Nonlinear Dynamics*, 2016,

83(1-2): 941–950.

33. Ju R, Fan W, Zhu W D, et al. A modified two-timescale incremental harmonic balance method for steady-state quasi-periodic responses of nonlinear systems. *Journal of Computational and Nonlinear Dynamics*, 2017, 12(5): 051007.
34. Cheung Y K, Chen S H, Lau S. Application of the incremental harmonic balance method to cubic non-linearity systems. *Journal of Sound and Vibration*, 1990, 140(2): 273–286.
35. Friedmann P, Hammond C E, Woo T H. Efficient numerical treatment of periodic systems with application to stability problems. *International Journal for Numerical Methods in Engineering*, 1977, 11(7): 1117–1136.